Research Square

Preprints are preliminary reports that have not undergone peer review.
They should not be considered conclusive, used to inform clinical practice,
or referenced by the media as validated information.

How multidimensional urban spatial agglomeration shapes carbon balance in seven Chinese megacities: Nonlinear relationships and geographic variations

Yan Chen
South China University of Technology
Sheng Jiao
jiaosheng2008@163.com

Hunan University
Zongcai Wei
State Key Laboratory of Subtropical Building Science
Xinyue Gu
Guangdong Academy of Sciences

Research Article

Keywords: Urban spatial agglomeration, Net carbon emissions, Nonlinear relationships, Geographically interpretable model, Spatial heterogeneity, Chinese megacities

Posted Date: November 18th, 2026

DOI: https://doi.org/10.21203/rs.3.rs-10661606/v1

License: This work is licensed under a Creative Commons Attribution 4.0 International License.
Read Full License

Additional Declarations: No competing interests reported.

How multidimensional urban spatial agglomeration shapes carbon balance in seven Chinese megacities: Nonlinear relationships and geographic variations

Yan Chen [a,b,c] , Sheng Jiao [c,d,e,*] , Zongcai Wei [a,b] , Xinyue Gu [f]

a State Key Laboratory of Subtropical Building and Urban Science, Guangzhou, 510641, China

b School of Architecture, South China University of Technology, Guangzhou, 510641, China

c College of Architecture and Planning, Hunan University, Changsha, 410082, China

d Hunan Key Laboratory of Sciences of Urban and Rural Human Settlements in Hilly Areas, Hunan University, Changsha 410082, China

e Hunan Engineering Technology Research Center for Smart Disaster Prevention and Resilient City Construction, Hunan University, Changsha 410082, China

f Guangzhou Institute of Geography, Guangdong Academy of Sciences, Guangzhou, 510070, China

* Corresponding author. jiaosheng2008@163.com (Sheng Jiao)

Abstract

Compact urban development has been widely considered a potential pathway for carbon mitigation, yet how different forms of urban spatial agglomeration influence urban carbon balance remains insufficiently understood. This study investigates the effects of multidimensional spatial agglomeration on net carbon emissions (NCE) in seven Chinese megacities by integrating multi-source geospatial data, ensemble learning, and interpretable spatial analysis. A spatially explicit carbon balance framework was developed by combining anthropogenic carbon emissions with terrestrial ecosystem carbon sequestration. Urban spatial agglomeration was quantified from three dimensions, including physical morphology, functional organization, and socioeconomic concentration, and their nonlinear relationships with urban carbon balance were further examined. The results reveal a clear spatial decoupling between carbon sources and sinks, with carbon emissions concentrated in urban cores and carbon sequestration mainly supported by peripheral ecological spaces. The effects of spatial agglomeration on carbon balance were nonlinear, with carbon impacts increasing during early stages of urban concentration but gradually weakening as improvements in resource efficiency and infrastructure sharing emerged. Among the agglomeration dimensions, socioeconomic and

functional clustering showed the strongest associations with NCE, whereas the carbon implications of urban morphology varied across geographic settings. Climate and topographic conditions further shaped these relationships by influencing energy demand, ecosystem productivity, and patterns of urban expansion. These findings suggest that the carbon implications of urban agglomeration depend on how urban activities, spatial structures, and ecological spaces are organized, rather than on compact development alone.

Keywords: Urban spatial agglomeration; Net carbon emissions; Nonlinear relationships; Geographically interpretable model; Spatial heterogeneity; Chinese megacities

1.Introduction

Climate change driven by anthropogenic carbon emissions has become one of the most pressing global challenges of the twenty-first century. Despite covering only 0.4%-0.9% of the Earth's land surface [1], urban areas consume nearly 80% of global energy and account for more than 70% of CO_2 emissions [2]. Megacities are particularly important emission hotspots due to their large populations, concentrated economic activities, and intensive energy demands [3]. Recent estimates suggest that the 100 largest urban agglomerations contribute nearly 18% of global CO_2 emissions [4]. Beyond their direct emissions, megacities influence surrounding regions through interconnected economic activities and environmental interactions [5]. These characteristics make megacities key arenas for climate mitigation and governance. Growing evidence from both research and planning practice suggests that optimizing urban spatial structures represents an important pathway toward low-carbon development [6]. Through land use optimization, low carbon infrastructure development, and ecological space conservation, spatial planning can contribute to climate mitigation and adaptation [7]. Therefore, identifying how spatial structures influence urban carbon outcomes is essential for developing effective climate strategies.

Urban spatial agglomeration is a key process through which urban activities, populations, and land uses become concentrated, thereby reshaping carbon emission and sequestration patterns. Existing studies have extensively

47 debated whether compact and concentrated urban development generates carbon benefits, but the underlying
48 mechanisms remain unresolved. On the one hand, agglomeration can reduce emissions by improving land-use
49 efficiency, shortening travel distances, and supporting public transport systems [8]. It may also reduce pressure on
50 surrounding ecological spaces by limiting urban expansion. On the other hand, excessive concentration can increase
51 carbon pressures through higher energy demand, traffic congestion [9], and reduced ecological capacity. Dense urban
52 forms may further modify local climatic conditions by intensifying heat accumulation and increasing building energy
53 consumption [10]. These contrasting findings indicate that the carbon consequences of urban spatial agglomeration
54 involve multiple interacting mechanisms that require further investigation.

55 The carbon effects of urban agglomeration cannot be fully understood through a single measure of urban
56 concentration because agglomeration involves multiple dimensions of urban organization. Existing studies have often
57 focused on individual aspects of urban form, functional structure, or socioeconomic concentration, providing valuable
58 insights but offering limited understanding of their combined effects on carbon outcomes. Physical agglomeration
59 reflects the spatial configuration of land uses and built environments, which influences energy consumption through
60 changes in density, ventilation, and thermal conditions [11]. Functional agglomeration captures how urban activities
61 are organized and connected, with factors such as land-use mix [12], job-housing balance [13], and polycentricity
62 [14] shaping mobility patterns and energy demand [15]. Socioeconomic agglomeration reflects the concentration of
63 population and economic activities, which can generate efficiency gains through agglomeration economies while
64 simultaneously increasing resource consumption and environmental pressures [16]. However, these dimensions are
65 often examined separately, leaving the integrated carbon consequences of urban agglomeration insufficiently
66 understood.

67 However, the carbon effects of urban agglomeration are not universal across geographic contexts. Local climatic
68 and topographic conditions regulate how spatial concentration influences both carbon emissions and ecosystem

carbon sequestration. Climate conditions modify the energy consequences of urban forms by affecting heating and cooling demands, as well as local climate zones (Zhang et al., 2015; Zhang et al., 2025). Meanwhile, climatic constraints on vegetation distribution, photosynthesis, and soil respiration determine the carbon sequestration capacity of urban ecosystems [19,20]. Topography further shapes these relationships by constraining urban expansion patterns, land-use configurations, and ecological conditions [21]. Therefore, understanding the carbon consequences of urban agglomeration requires considering not only how cities are organized internally but also how these spatial processes interact with regional environmental contexts.

Despite growing efforts to understand the carbon consequences of urban spatial agglomeration, existing studies have largely examined individual aspects of urban spatial organization or focused on emissions alone. Such approaches provide limited understanding of how multiple spatial processes jointly shape net carbon outcomes and why these relationships vary across geographic contexts. To address these gaps, this study focuses on three questions: (1) How do multidimensional forms of urban spatial agglomeration shape net carbon emissions in Chinese megacities? (2) How do different dimensions of urban spatial agglomeration contribute to variations in net carbon outcomes? (3) How do climatic and topographic contexts modify these carbon effects?

Taking Chinese seven megacities as a case study, this research investigates how multidimensional urban spatial agglomeration shapes net carbon emissions under diverse geographic contexts. Chinese megacities provide a suitable setting for this analysis because they combine intensive human activities with substantial variations in climatic and topographic conditions. To address the research questions, we integrate multi-source data, including social sensing data, nighttime light imagery, and population density, to estimate high-resolution anthropogenic carbon emissions and combine them with net ecosystem productivity (NEP) to construct spatially explicit net carbon emissions (NCE). We further develop a multidimensional framework of urban spatial agglomeration encompassing physical, functional, and socioeconomic dimensions and apply a geographically interpretable machine learning framework to identify

nonlinear and spatially heterogeneous carbon responses under different geographic conditions.

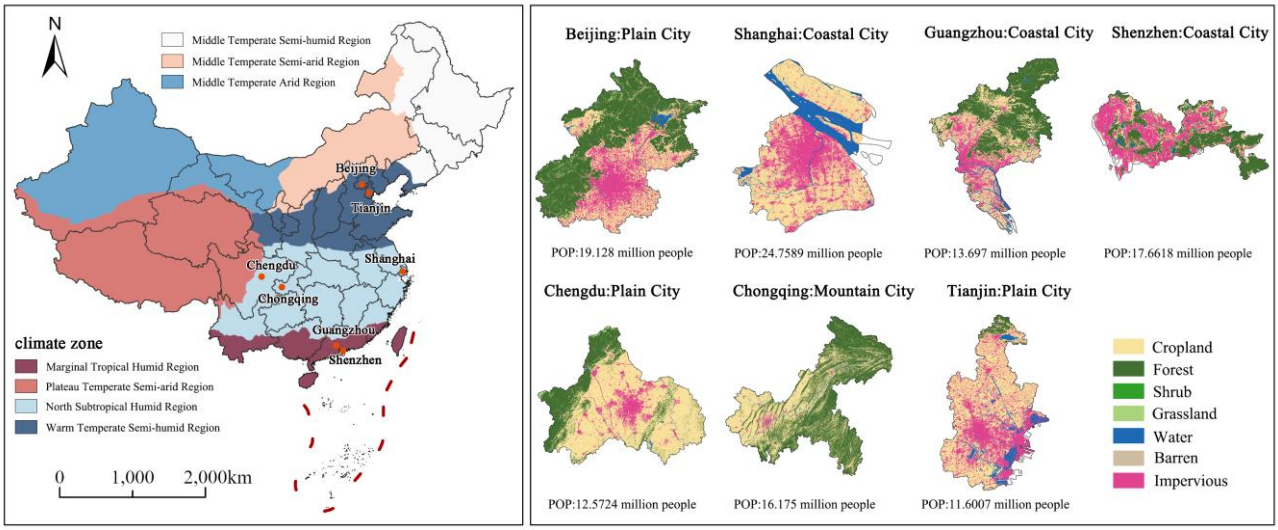
This study makes three main contributions. First, it develops a high-resolution urban carbon assessment approach by integrating multi-source geospatial data to quantify both anthropogenic carbon emissions and terrestrial ecosystem carbon sequestration. This approach provides a more comprehensive understanding of urban carbon balance by considering both carbon sources and sinks. Second, it extends existing urban agglomeration research beyond single-dimensional measurements by examining how physical, functional, and socioeconomic forms of spatial agglomeration affect net carbon emissions. This multidimensional perspective helps clarify the differentiated carbon effects associated with different aspects of urban agglomeration. Third, it advances the geographic understanding of urban spatial agglomeration by incorporating climatic and topographic contexts into the analysis of carbon effects. Collectively, these contributions provide a more comprehensive perspective on how urban spatial organization influences carbon balance and offer scientific support for developing targeted low-carbon planning strategies in megacities.

2.Methods

2.1 Study area

This study selected seven megacities in China, including Shanghai, Beijing, Shenzhen, Chongqing, Guangzhou, Chengdu, and Tianjin, based on the urban classification criteria defined by China's Seventh National Population Census (Fig. 1). All districts within the administrative boundaries of each megacity were included in the analysis. These megacities provide a suitable context for examining the relationship between urban spatial agglomeration and net carbon emissions under diverse geographic conditions. Geographically, the selected megacities span a broad climatic gradient, covering warm temperate semi-humid, northern subtropical humid, and marginal tropical humid zones. Such climatic diversity results in variations in urban energy demand and ecosystem carbon sequestration capacity. In addition to climatic differences, these megacities also exhibit substantial topographic heterogeneity,

ranging from plains and coastal lowlands to mountainous regions, which imposes different constraints on urban development and ecological processes.



(a)Map of China (b)Study area of seven megacities

Fig.1. The distribution of study areas.

2.2 Methodological framework

In this study, the research process was structured into four main components (Fig. 2). First, we conducted net carbon emission accounting and harmonized multi-source datasets. Second, we performed spatial autocorrelation and multicollinearity tests on the selected variables to ensure the robustness of their mathematical relationships, and subsequently developed an ensemble learning framework based on multiple base learners. Third, we applied the Geographically interpretable framework to incorporate geographic features, examining how spatial clustering across multiple dimensions contributes to urban net carbon emissions. Finally, we analyzed city categories defined by climatic zones and topography to identify variations in the impact of spatial clustering, thereby providing insights for low-carbon urban development.

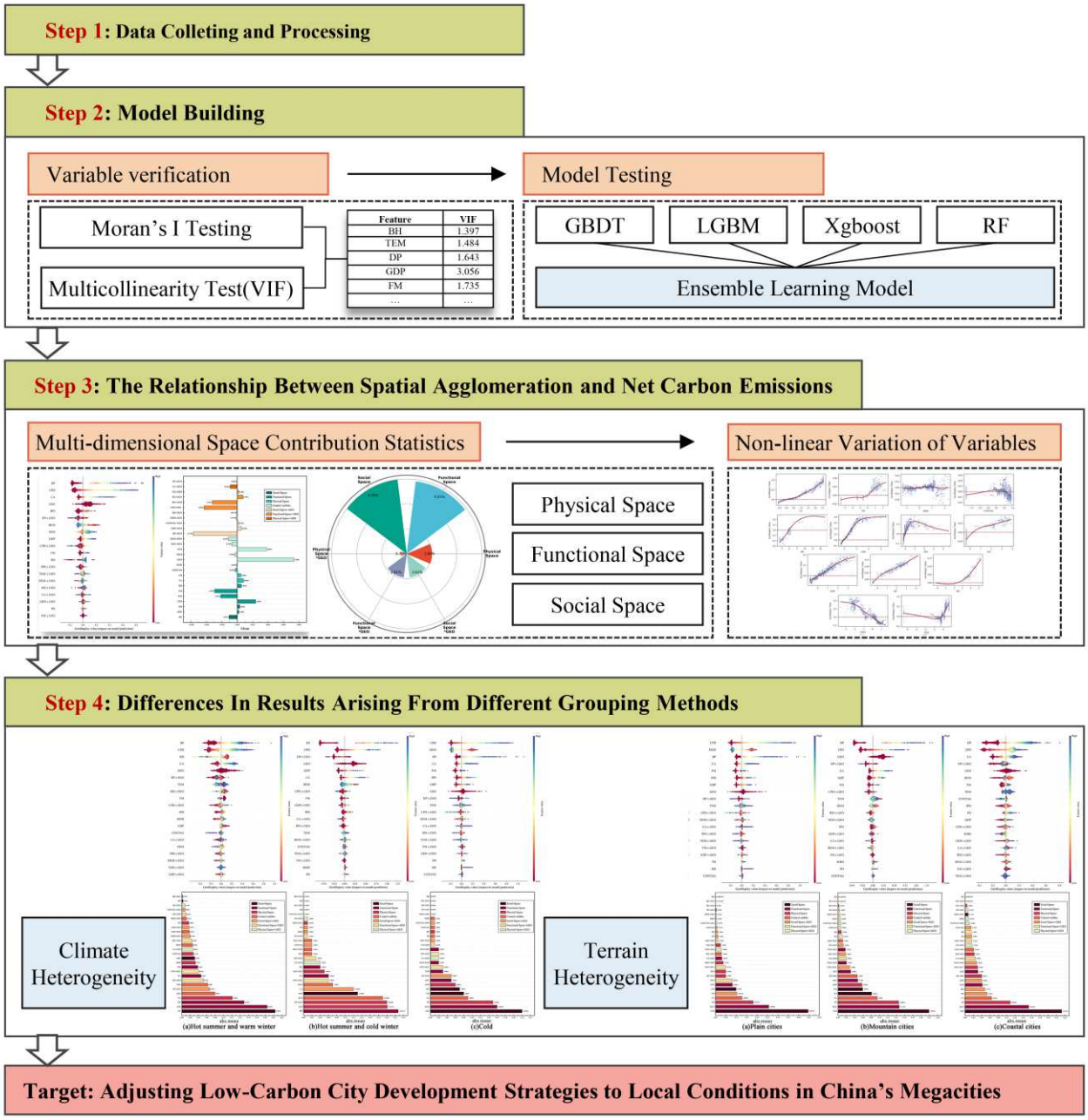


Fig.2. Methodological framework

2.3 Data source

To ensure data consistency, all datasets used in this study were collected for 2022 and analyzed within the administrative boundaries of the selected megacities. Multiple data sources were integrated to characterize urban activities, spatial functions, and environmental conditions. Geotagged check-in data from Sina Weibo were obtained using a custom-built web crawler, covering the period from January 1 to December 31, 2022. The dataset includes

timestamps, textual information, geographic coordinates, and associated images. After data cleaning, including deduplication, coordinate validation, and removal of irrelevant records, 2,816,238 valid observations were retained for subsequent analysis. Point-of-interest (POI) data were obtained through the Gaode Map API and reclassified according to the Standard for Classification of Urban Land Use and Planning of Construction Land (GB 50137-2011) to ensure consistency between POI categories and standardized land-use functions. All spatial datasets were processed in ArcGIS Pro 3.0.2 and projected to the WGS_1984_Albers coordinate system. To ensure spatial consistency across datasets, all layers were resampled and converted into raster grids with a spatial resolution of 500 m. Variables derived from different data sources were normalized using a logarithmic transformation followed by Z-score standardization to reduce scale differences. Detailed information on data sources, spatial resolution, and acquisition methods is summarized in Table 1.

Table 1 Summary of data sources.

Class	Description	Resolution	Release Date	Source
Land use	/	30m, raster	2022	https://zenodo.org/records/12779975
Statistical	Carbon emissions from EDGAR	Table	2022	https://edgar.jrc.ec.europa.eu/
Satellite image	Nighttime light	250m, raster	2022	[22]
Social media	Weibo check-in location	Table	2022.01.01-2022.12.31	https://www.weibo.com
Socioeconomic	Population	1 km, raster	2022	https://www.resdc.cn/
	Gridded GDP	Table	2020	https://www.resdc.cn/
	POI	Vector	2022	www.lbs.amap. com/
	Road	1 km, raster	2022	https://osm.mapplus.cn/
	Building height	10m, raster	2020	[23]
Physical geography	Temperature	1 km, raster	2022	www.gis5g.com
	Precipitation	1 km, raster	2022	tpdc.ac.cn
	Elevation	500 m, raster	2022	https://www.ncei.noaa.gov/products/etopo-global-relief-model
	NPP	500 m, raster	2022	www.gis5g.com
	SOC	1 km, raster	2019	https://www.fao.org
	Climate zones	Vector	2005	https://gitcode.com/open-source-toolkit/1849d
Boundary	Administrative zoning	Vector	2022	www.tianditu. gov.cn

2.4 Methodology

2.4.1 Selection of study variables

Based on the theoretical framework of urban spatial agglomeration and carbon processes, this study establishes a variable system consisting of the dependent variable, explanatory variables, control variables, and grouping variables (Table 2).

(1) Dependent variable

Net carbon emissions (NCE) served as the dependent variable in this study. In the calculation, anthropogenic carbon emissions and terrestrial vegetation carbon sequestration were incorporated into the accounting framework, with the specific computational procedure illustrated in Figure 3.

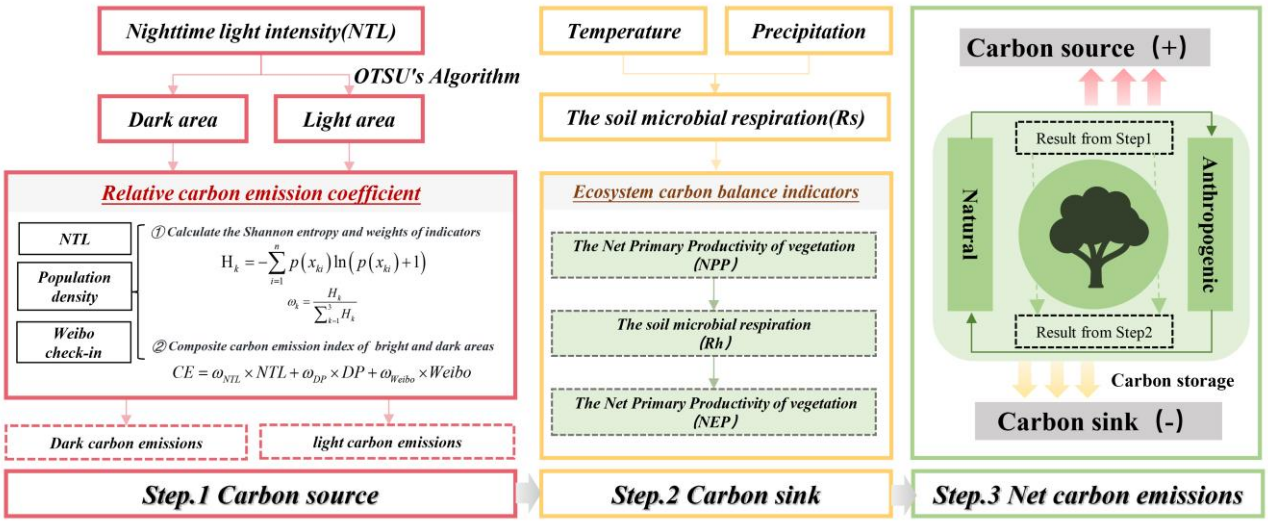


Fig.3. The workflow of the spatially explicit net carbon emissions.

(i) Carbon source calculation

To effectively differentiate between bright urban areas and dark background regions in nighttime light imagery, this study employs the OTSU algorithm to automatically calculate the optimal brightness threshold, thereby achieving image binarization. The core of this algorithm is to find the optimal threshold T that maximizes the between-class variance σ_B^2 between the foreground and background after segmentation. The calculation formula is as follows:

$$\sigma_B^2(T) = \omega_0(T) \cdot \omega_1(T) \cdot [\mu_0(T) - \mu_1(T)]^2 \quad (1)$$

Where ω_0 and ω_1 represent the proportions of dark and bright region pixels segmented by the threshold T, and μ_0 and μ_1 represent the corresponding average grayscale values. By iterating over all possible grayscale levels, the threshold T^* that maximizes σ_B^2 (T) is selected as the optimal segmentation threshold:

$$T^* = \underset{T}{argmax}(\sigma_B^2(T)) \quad (2)$$

The original image is converted to a binary mask using T^*, where pixels with a brightness value higher than T^* are identified as "bright areas", operationally defined as agricultural production emissions; conversely, pixels with lower brightness are considered "dark areas", encompassing energy consumption, industrial processes, and product usage emissions, which are quantified using EDGAR v2024 data (Table S1).

Spatial allocation was performed using grid-level weights combining NTL intensity, population density, and geo-tagged social media check-in density, yielding emissions in metric tons per square kilometer (mt/km²):

$$H_k = -\sum_{i=1}^{n} p(x_{ki}) \ln(p(x_{ki}) + 1) \quad (3)$$

$$\omega_k = \frac{H_k}{\sum_{i=1}^{3} H_k} \quad (4)$$

$$\begin{cases} RCE_L = \sum_{i=1}^{3} \omega_k x_{ki} \\ RCE_D = \sum_{i=1}^{3} \omega_k x_{ki} \end{cases} \quad (5)$$

Where H_k denotes the Shannon entropy index for indicator category k, and x_{ki} represents the spatial metrics of category k, with $p(x_{ki})$ representing the normalized probability distribution of the spatial metrics. ω_k is the weight for the k-th indicator, and RCE_L and RCE_D represent the spatial carbon emissions of the bright and dark areas, respectively.

(ii) Carbon sink calculation

Subsequently, net ecosystem productivity (NEP) serves as the carbon sink metric [24]:

$$NEP = NPP - R_h \quad (6)$$

where NPP denotes net primary productivity (kg C·m^{-2}·a^{-1}) and R_h represents heterotrophic respiration. Annual soil respiration (R_s) is computed via a temperature-precipitation regression model:

$$R_h = 0.6163 R_s^{0.7981} \quad (7)$$

$$R_s = 1.55 e^{0.031T} \times \frac{P}{P + 0.68} \times \frac{SOC}{SOC + 2.23} \quad (8)$$

with T as mean annual temperature (°C), P as annual precipitation (m), and SOC as surface soil organic carbon density (0-20 cm layer, kg/m²).

Finally, the NCE metric integrates anthropogenic and natural carbon fluxes:

$$NCE_n = CE_n - NEP_n \quad (9)$$

where CE_n and NEP_n denote normalized anthropogenic emissions and natural carbon sequestration, respectively. Positive NCE values indicate carbon deficit (net sources), while negative values signify carbon surplus (net sinks).

(2) Independent variables

Based on the concept of urban spatial agglomeration, this study develops an explanatory variable system encompassing physical, functional, and socioeconomic dimensions. The selection of dimensions and indicators follows two principles: (1) capturing the major processes through which urban activities are concentrated and organized, and (2) ensuring consistency with established measurements of urban spatial structure. Specifically, the physical dimension characterizes the morphological configuration of urban space, the functional dimension reflects the organization and interaction of urban activities, and the socioeconomic dimension represents the concentration intensity of population and economic resources.

The physical dimension is measured using landscape metrics, including Class Area (CA), Patch Density (PD), Shannon's Diversity Index (SHDI), and Contagion Index (CONTAG), which capture the density, aggregation, and diversity of urban land-use patterns [25]. Road density is additionally included to represent spatial connectivity. The

functional dimension is characterized by the spatial concentration of commercial and industrial activities derived from POI data and functional diversity measured using information entropy. The socioeconomic dimension is represented by population density, GDP, and building height, reflecting population concentration, economic intensity, and vertical urban development [26].

(3) Control variables

This study also incorporates several control variables that may influence NCE, specifically temperature, topography, and geographical coordinates. Temperature affects the carbon cycle by shaping ecosystem respiration and energy consumption patterns. Topography indirectly influences carbon emissions through its effects on vegetation distribution and modes of human activity. Geographical coordinates are included to capture spatial heterogeneity, and their contribution is quantified within the geographically interpretable model.

(4) Grouping Variables

Climate and topographic zones were employed as grouping variables. To elucidate the relationship between buildings and climate, [27] divides China into seven primary building climate zones. In addition, cities are classified by topographic features of urban construction land. Accordingly, this study adopts both climate and topographic zones, as defined in the Chinese standards for urban construction, to capture the influence of urban type heterogeneity on the analysis results.

2.4.2 Ensemble learning model construction

To capture nonlinear relationships between urban spatial agglomeration and NCE, this study developed a weighted ensemble learning framework (WEL) integrating LightGBM, XGBoost, GBDT, and Random Forest. Each base learner was trained with randomized hyperparameters to enhance model diversity. Model weights were assigned according to validation (R^2), allowing models with stronger explanatory performance to contribute more to the ensemble prediction (Fig. S1; Table S3-4). The final prediction was calculated as:

$$\hat{y} = \sum_{i=1}^{4} \left(\frac{R_i^2}{\sum_{i=1}^{4} R_i^2} \right) \hat{y}_i \tag{11}$$

where $\hat{y}_i$ and R_i^2 denote the prediction and validation R^2 score of the i-th base model. This weighting strategy improves model robustness while maintaining ensemble diversity.

2.4.3 Explanatory models for measuring spatial effects (Geoshapley)

Although machine learning models can capture complex nonlinear relationships, their interpretation of spatial processes remains limited. Therefore, GeoShapley was applied to quantify location-dependent feature contributions by incorporating geographic coordinates into the SHAP framework. In this approach, geographic coordinates were treated as a composite feature (GEO), and their interactions with other predictors were decomposed using Shapley values. The model prediction was separated into four components:

$$\hat{y} = \varphi_0 + \varphi_{GEO} + \sum_{j=1}^{p} \varphi_j + \sum_{j=1}^{p} \varphi_{(GEO,j)} \tag{12}$$

where (1) φ_0 : Global intercept (mean prediction over background samples); (2) φ_{GEO} : Intrinsic spatial effect of pixel centroids; (3) φ_j : Location-invariant contribution of feature j; and (4) $\varphi_{(GEO,j)}$: Spatially varying interaction between feature j and coordinates. The spatial effect φ_{GEO} is computed as:

$$\varphi_{GEO} = \sum_{S \subseteq N \setminus \{GEO,j\}} \frac{|S|!\left(|N| - |S| - g\right)!}{\left(|N| - g + 1\right)!} \left(V\left(S \cup \{GEO\}\right) - V(S) \right) \tag{13}$$

where N denotes all features, g the dimensionality of GEO coordinates, and $V(S)$ the characteristic function. Feature interaction terms $\varphi_{(GEO,j)}$ follow the Shapley interaction index formalism:

$$\varphi_{GEO} = \sum_{S \subseteq N \setminus \{GEO,j\}} \frac{|S|!\left(|N| - |S| - g\right)!}{\left(|N| - g + 1\right)!} \Delta_{\{GEO,j\}} \tag{14}$$

$$\Delta_{\{GEO,j\}} = V\left(S \cup \{GEO, j\}\right) - V\left(S \cup \{GEO\}\right) - V\left(S \cup \{j\}\right) + V(S) \tag{15}$$

To improve computational efficiency for large-scale spatial analysis, a stratified sampling strategy based on k-means clustering was applied following [28]. Sensitivity tests indicated that 1,000 representative samples provided a

224 balance between computational efficiency and spatial interpretability (Fig. S2-3; Table S5). Geographic coordinates

225 were represented using projected pixel centroids in the WGS_1984_Albers system.

226

Table 2 Evaluation index system for spatial agglomeration in megacities

Target layer	System layer	Indicator layer	Abbreviation	Year	Units	Definition
Explained variables	/	Net carbon emissions	NCE	2022	mt	The difference between anthropogenic carbon emissions and terrestrial carbon sequestration.
Response variables	Physical space: urban morphological structure aggregation	Urban construction land area	CA	2022	km^2	Total land area allocated for urban development, covering residential, commercial, industrial, and infrastructure uses
		Patch density	PD	2022	square/km^2	Number of patches per unit area, indicating landscape heterogeneity and fragmentation
		Shannon's diversity index	SHDI	2022	/	Composite metric reflecting landscape diversity and evenness
		Contagion index	CONTAG	2022	%	Degree of aggregation or spatial spread of distinct patch types in a landscape
		Road density	RD	2022	km/km^2	Total length of roads per unit area, measuring coverage and connectivity of transportation infrastructure
	Functional space: urban element aggregation	Commercial facility density	CPD	2022	points/km^2	Number of commercial and service facilities per unit area, indicating service accessibility and regional commercial activity intensity
		Industrial facility density	IPD	2022	points/km^2	Number of industrial facilities per unit area, reflecting production capacity concentration and regional industrialization level
		Functional diversity	FM	2022	/	Metric quantifying the mix of urban facilities using the Shannon Index, reflecting functional balance and land-use heterogeneity
	Social space: socio-economic aggregation	Gross domestic product	GDP	2020	Million yuan	Spatial pattern of economic output across regions, reflecting concentration of economic activity and inter-regional disparities
		Population density	DP	2022	persons	Spatial pattern of population distribution, measured as the number of individuals per unit area, reflecting human settlement concentration and regional carrying capacity.
		Building height	BH	2020	m	Vertical dimension of structures, typically measured in meters, indicating urban vertical expansion intensity and spatial efficiency
	Natural factor	Temperature	TEM	2022	℃	Annual mean temperature (monthly averages)
		Elevation	DEM	2022	m	Surface altitude data
Control variables	Geographic factor	Longitude	LON	/	°	The horizontal coordinate of the spherical coordinate system
		Latitude	LAT	/	°	The vertical coordinate of the spherical coordinate system
Spatial grouping variables	/	Climatic zones	/	/	/	Seven bioclimatic regions aligned with China GB50176–93
	/	Topographic zones	/	/	/	The classification of Chinese cities is based on the geographic settings, topographical features, and spatial distribution patterns

227 # 3.Results

228 The results are organized around four analytical steps. We first describe the spatial patterns of carbon sources,

229 carbon sinks, and net carbon balance across China's megacities. We then examine the spatial dependence of net

230 carbon emissions and compare the performance of different regression models. Next, we identify the main variables

contributing to carbon outcomes and assess their marginal effects. Finally, we examine how these contributions vary across different climatic and topographic settings.

3.1 Spatial mismatch between carbon sources and sinks in Chinese megacities

3.1.1 Spatial concentration of carbon sources

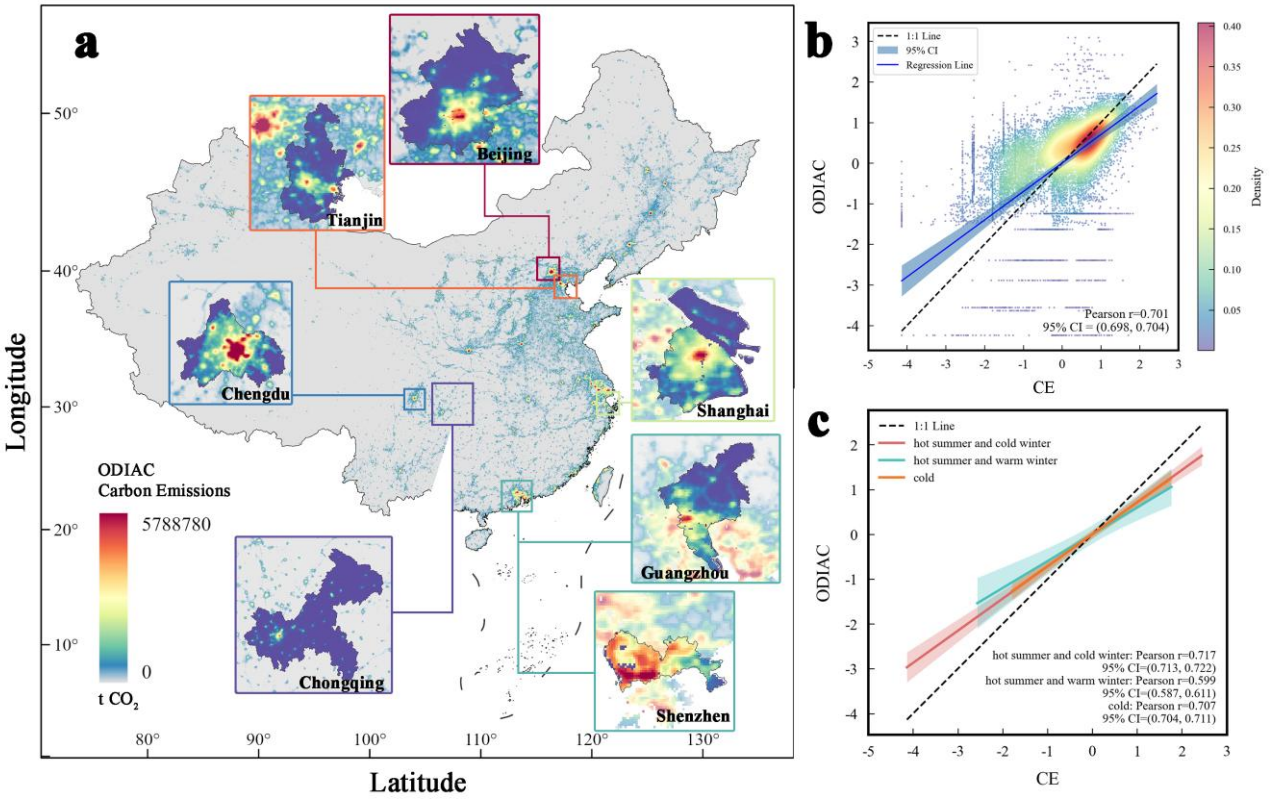


Fig.4. Correlation test between carbon source estimates and ODIAC.

The estimated carbon emissions showed strong consistency with ODIAC, with a significant correlation after harmonizing both datasets at a 500 m spatial resolution (Pearson's r = 0.701, p = 0.001; Fig. 4). The two datasets exhibited similar spatial patterns across different climatic zones and along spatial gradients, indicating that the proposed estimation approach successfully captured the overall distribution of anthropogenic carbon emissions. However, differences emerged within densely developed urban areas, where our estimates identified more detailed emission variations than ODIAC. This improvement likely results from the integration of multiple spatial indicators, including nighttime light intensity, population density, and social sensing data, which helps reduce the uncertainty

associated with relying on a single remote sensing source. Therefore, the estimated emissions provide a reliable basis for examining the spatial relationship between urban spatial agglomeration and net carbon balance.

Anthropogenic carbon emissions in China's megacities generally declined from intensively built-up areas toward the urban periphery. The concentric-ring analysis in Fig. 5(1a-g) shows that emission intensity was generally higher in the administrative core and surrounding built-up areas of the seven cities, and decreased with distance from these areas. This pattern indicates that high-emission activities were concentrated in urban spaces with greater development intensity and denser human activity, whereas peripheral areas had relatively lower emission intensity. Within this broad gradient, emission hotspots were mainly associated with central business districts, major urban centers, large transportation hubs, and industrial clusters. Commercial and administrative centers tended to form continuous high-emission cores, while airports, ports, and high-speed railway stations appeared as localized hotspots. Industrial clusters were more dispersed and were usually located outside the central urban area. Together, these functional spaces formed the main hotspot structure of carbon emissions in the megacities.

Within this general distance-decay pattern, the concentration and direction of high-emission areas varied across cities. In Beijing, Tianjin, Guangzhou, and Chengdu, high-emission areas were mainly organized around the main urban districts, producing a relatively concentric pattern. By contrast, Shanghai and Shenzhen showed a more dispersed high-value structure, with emission hotspots extending from the central urban area toward peripheral industrial spaces, transport nodes, and port-related areas. This pattern indicates a more evident polycentric structure. Chongqing showed a stronger directional pattern, with high-emission areas concentrated in the western central urban area and extending east-west along the Yangtze River system. This produced a corridor-like and clustered distribution. Overall, the seven megacities shared a similar distance-decay tendency, but differed in the spatial organization of high emission areas.

3.1.2 Peripheral distribution of carbon sinks

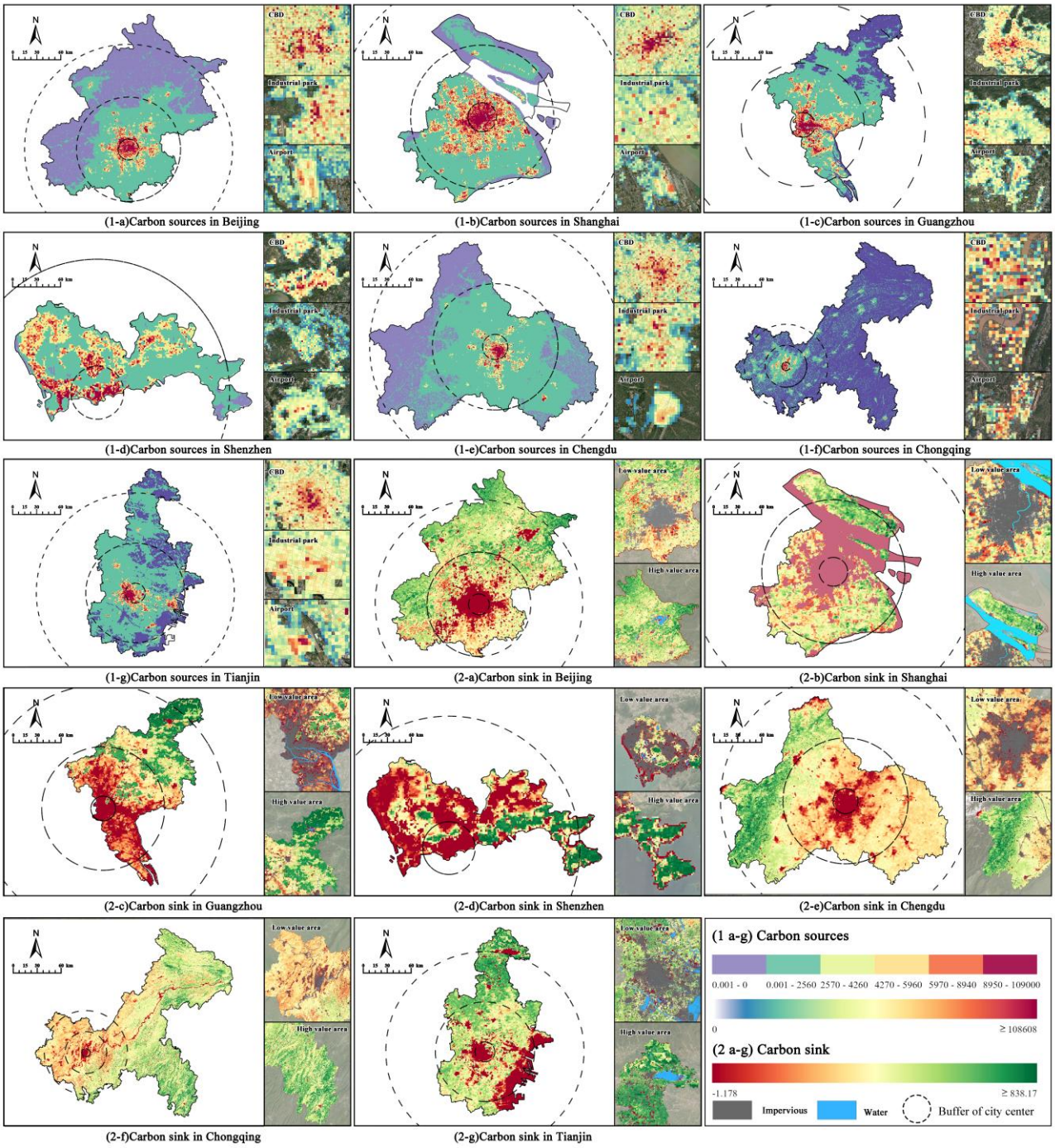


Fig.5. Spatial distribution of carbon sources and sinks in seven Chinese megacities.

Notes: Three buffers with radii of 10 km, 50km and 100 km show the extent of sample cities.

Vegetation carbon sinks in the megacities were concentrated mainly in peripheral areas. Fig. 5(2a-g) shows that carbon sink capacity was generally weak in the central built-up areas of the seven cities. Some intensively developed areas even showed negative NEP values, indicating a shift from carbon sink to carbon source. By contrast, high sink

values were mainly found 50-100 km from the city center. These areas broadly corresponded to continuous vegetation cover, forests, and agricultural ecosystems, whereas low-value areas were mostly associated with dense built-up land. Thus, vegetation carbon sinks in the megacities were mainly supported by peripheral ecological spaces, especially in gently sloping mountainous areas.

Differences in carbon sink patterns among cities were closely related to climatic background and topographic conditions. Chongqing and Chengdu are located in humid climate zones and have extensive peripheral mountains, hills, and vegetated areas, which corresponded to broader high-value sink areas. Shenzhen and Guangzhou are also located in warm and humid southern China, but their main built-up areas lie on coastal plains and river-delta landscapes, where low sink values overlapped strongly with intensively developed land. In flatter cities such as Beijing, Tianjin, and Shanghai, high sink values were mainly found in peripheral farmland and forested areas, while carbon sink capacity remained limited in the central built-up areas. Overall, climate and topography jointly shaped the spatial differences in vegetation carbon sinks across the megacities.

3.1.3 Net carbon emissions patterns across cities and natural settings

Net carbon emissions (NCE) varied considerably among the seven megacities, reflecting differences in the relationship between anthropogenic emissions and ecosystem carbon sequestration. Beijing showed a predominantly net-emission pattern, with NCE values concentrated in the medium-to-high range. In contrast, Chengdu and Chongqing exhibited wider distributions of negative NCE values, indicating a stronger contribution of carbon sequestration to offsetting emissions. Shanghai and Shenzhen displayed bimodal NCE distributions, with both high and low values occurring within the urban areas, suggesting a spatial separation between emission-intensive zones and carbon sink areas.

The distribution of NCE also varied across climatic and topographic settings. Cities in cold climate zones showed relatively narrow NCE ranges, whereas cities in hot-summer cold-winter and hot-summer warm-winter zones

exhibited greater variability. Mountain cities generally showed wider ranges of negative NCE values, while coastal cities presented stronger contrasts between carbon source and sink areas. Overall, variations in urban net carbon balance were associated with differences in urban development patterns and ecological carbon sequestration, with geographic settings contributing to these spatial variations.

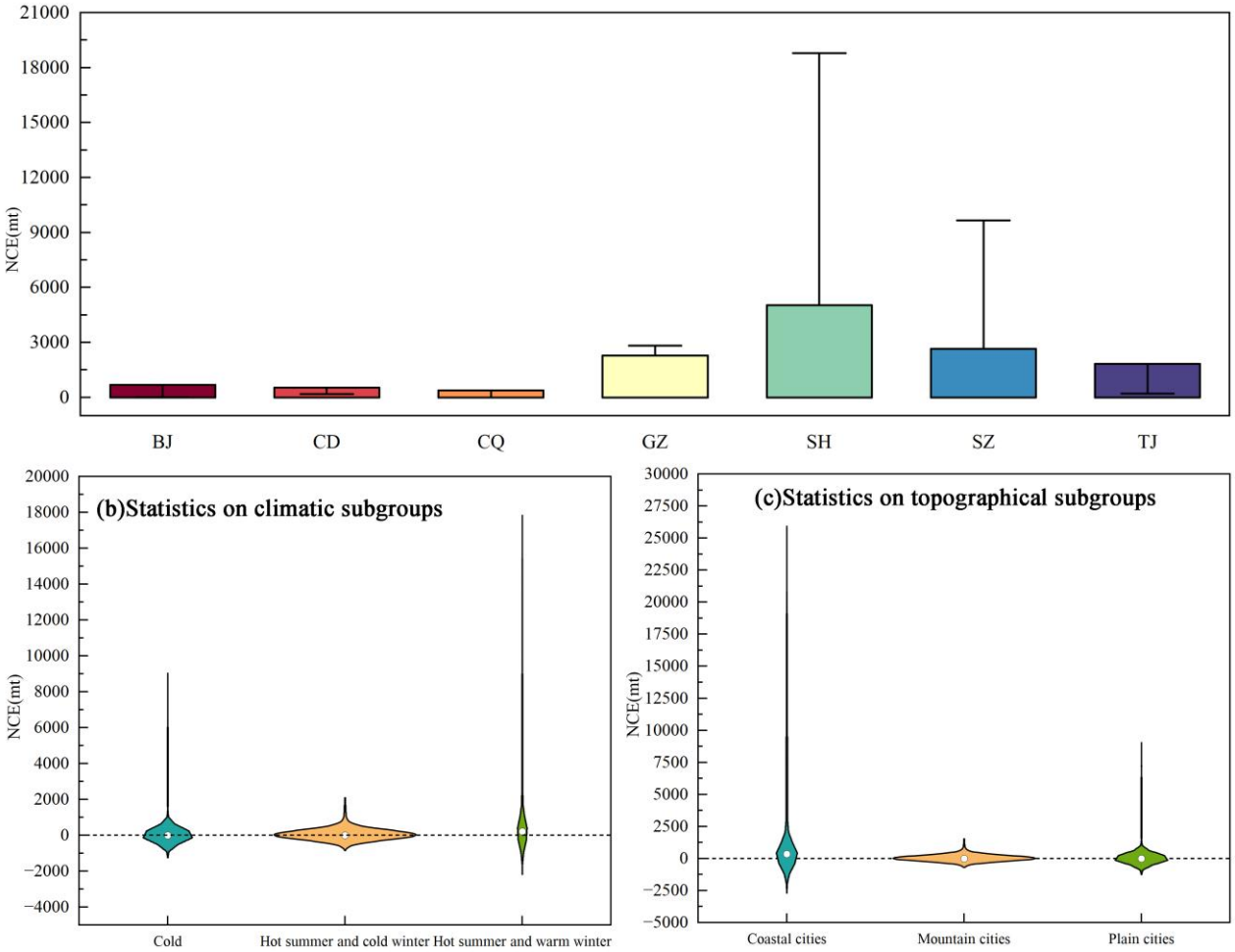


Fig.6. Violin plots of NCE in (a) Chinese megacities, (b) climate zones, and (c) topographical subgroups.

3.2 Spatial dependence and model performance

The Moran's I result show that NCE was positively spatially autocorrelated in all seven megacities (Table 3). This pattern is consistent with the clustered distributions of carbon sources and sinks described above, and indicates that net carbon emissions were not randomly distributed across urban space. The VIF results further suggest that most explanatory variables had acceptable levels of collinearity (Table 4). These tests support the need for regression

models that can account for spatially structured and potentially nonlinear relationships.

Table 3 Global Moran's I of NCE in seven Chinese Megacities.

City	Moran'I	p-value
Beijing	0.943	0.001
Chengdu	0.860	0.001
Chongqing	0.639	0.001
Guangzhou	0.829	0.001
Shanghai	0.887	0.001
Shenzhen	0.878	0.001
Tianjin	0.886	0.001

Table 4 Test for multicollinearity of variables.

Feature	VIF	Feature	VIF
BH	1.397	CONTAG	1.864
TEM	1.484	CA	3.976
DP	1.643	PD	4.095
GDP	3.056	SHDI	3.041
FM	1.735	LAT	3.853
CPD	6.223	LON	2.498
IPD	3.735	RD	1.146
DEM	3.272		

Model performance was compared across linear, nonlinear, and ensemble regression approaches using R^2, MSE, and MAE (Table 5). The nonlinear models clearly outperformed OLS, suggesting that the relationship between urban agglomeration factors and NCE is better represented by nonlinear specifications. Although some individual tree-based models achieved slightly higher training accuracy, their train-test gaps were larger. By contrast, the weighted ensemble model showed a more balanced performance between the training and testing sets, with consistently low MSE and MAE. This stability makes the ensemble model a more reliable basis for interpreting variable contributions in the following analysis.

Table 5 Global dataset evaluation metrics for machine-learning models.

Model	R^2 score		Mean Squared Error		Mean Absolute Error	
	Training set	Testing set	Training set	Testing set	Training set	Testing set
OLS	0.708	0.708	0.292	0.292	0.418	0.418

GBDT	0.898	0.897	0.102	0.103	0.191	0.192
XGBoost	0.918	0.915	0.082	0.085	0.165	0.168
LGBM	0.932	0.927	0.068	0.073	0.151	0.155
RF	0.963	0.949	0.037	0.051	0.110	0.129
Blended	0.934	0.927	0.066	0.073	0.150	0.156

3.3 Variable contributions and marginal effects

3.3.1 Main contributors to carbon outcomes

The GeoShapley results show that socioeconomic concentration and urban functional agglomeration were key factors in explaining net carbon emissions (NCE). Figures 7 and 8 show that population density (DP) had the largest contribution, accounting for 19.74% of the model explanation. This indicates that areas with higher population concentration tended to have higher NCE. Functional agglomeration also played an important role. Commercial facility density (CPD) and industrial enterprise density (IPD) contributed 17.76% and 6.59%, respectively. These results suggest that NCE was shaped not only by population concentration, but also by the spatial clustering of commercial and industrial activities. Construction area (CA) contributed 9.34%, further indicating the role of horizontal expansion of built-up space. By contrast, building height (BH) contributed only 0.31%, suggesting a limited direct effect of vertical urban form. Overall, the spatial variation in NCE was explained mainly by the horizontal concentration of urban spatial elements, while vertical form played a much smaller role.

Geographic location and natural conditions further shaped the context in which urban agglomeration affected NCE. GEO contributed 8.12%, which was lower than the contributions of population density and commercial facility density but higher than those of several morphological and natural variables. This suggests that spatial location had a moderate role in the model explanation. The GeoShapley results further show that, after controlling for other variables, different locations were associated with different directions of change in NCE. In other words, similar agglomeration characteristics could produce different net carbon outcomes depending on where they occurred. This location effect was also reflected in variable interactions. GEO amplified the effect of SHDI on NCE, suggesting that

the role of land-use diversity depended partly on spatial location. DEM and TEM contributed 6.39% and 5.03%, respectively, indicating that topography and climate also contributed to the spatial differentiation of NCE. Overall, the explanatory structure of NCE reflected both the concentration of urban elements and the geographic and natural settings in which these elements were embedded.

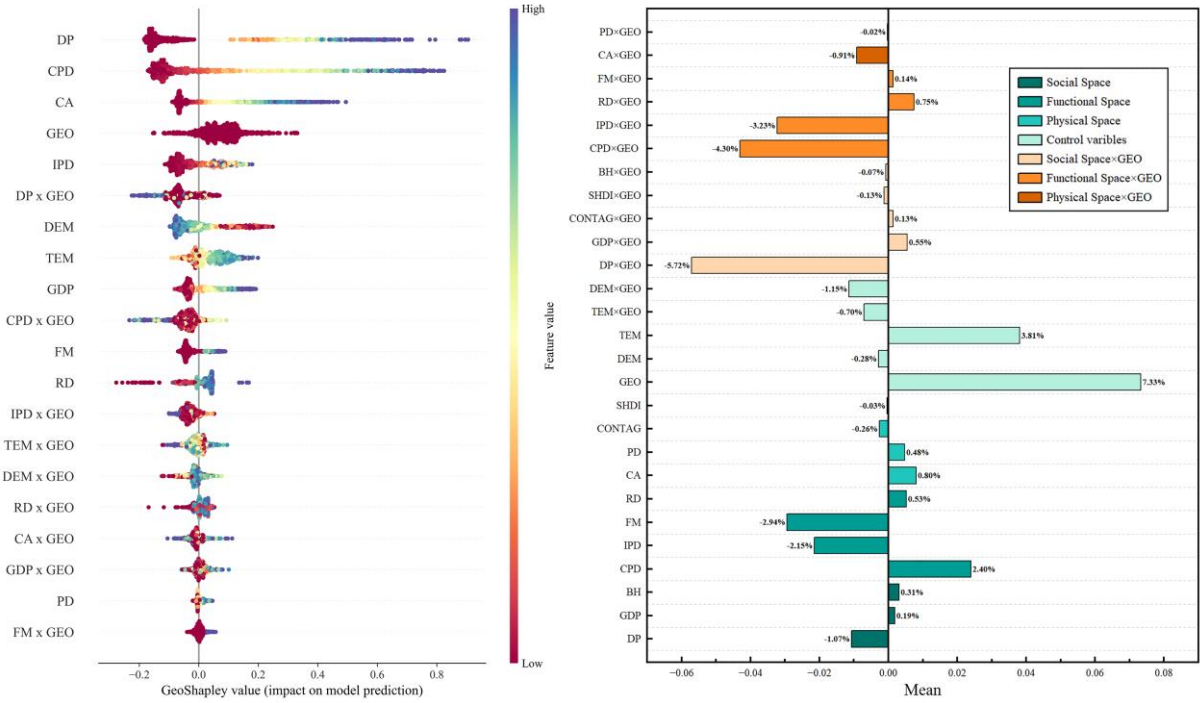


Fig.7. Global interpretation of feature effects on NCE.

Notes: For specific Geoshapley values, see Table S6.

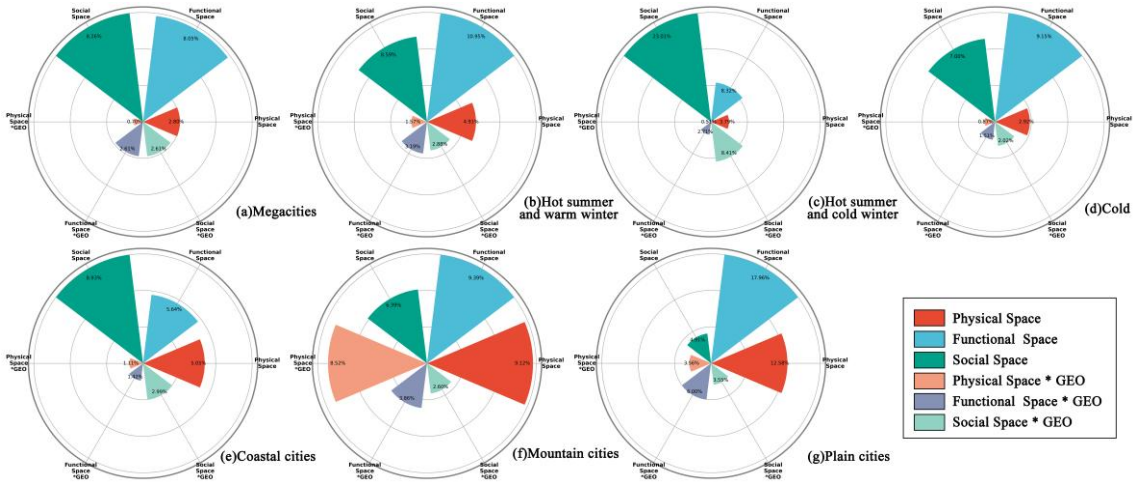


Fig.8. Contribution of multiple spatial agglomerations to NCE.

3.3.2 Marginal effects of explanatory variables

The marginal effect results show that different types of variables were associated with different response patterns in NCE. As shown in Fig. 9, scale-related variables, including construction area (CA), GDP, population density (DP), and building height (BH), showed steadily increasing marginal contributions as their values increased. This indicates that larger urban scale and higher activity intensity were associated with higher NCE levels. By contrast, spatial organization variables, including road density (RD), commercial facility density (CPD), patch density (PD), and functional mix (FM), tended to level off after reaching a certain range. Their effects on NCE therefore did not increase linearly. Industrial enterprise density (IPD) showed an inverted U-shaped relationship, with its marginal contribution declining after a relative value of approximately 2.0. This pattern indicates a threshold effect in the relationship between industrial agglomeration and NCE. The marginal effects of the landscape metrics SHDI and CONTAG were relatively stable, suggesting a weaker or more indirect response. Overall, scale-related variables showed a cumulative increase in their effects, whereas spatial organization variables were more likely to exhibit plateaus or threshold responses.

Natural variables showed response patterns that differed from those of urban agglomeration variables. Temperature (TEM) had a U-shaped relationship with NCE. When the relative temperature was below -1, NCE remained relatively low; as the temperature increased, the marginal contribution of TEM also increased. Elevation (DEM), by contrast, showed a negative relationship with NCE, with higher DEM values corresponding to lower NCE levels. Compared with urban scale and functional variables, natural variables did not show a simple monotonic agglomeration effect. Instead, their effects varied across temperature ranges and elevation gradients. These results suggest that the marginal response of NCE is shaped not only by urban expansion and spatial organization, but also by natural geographic conditions.

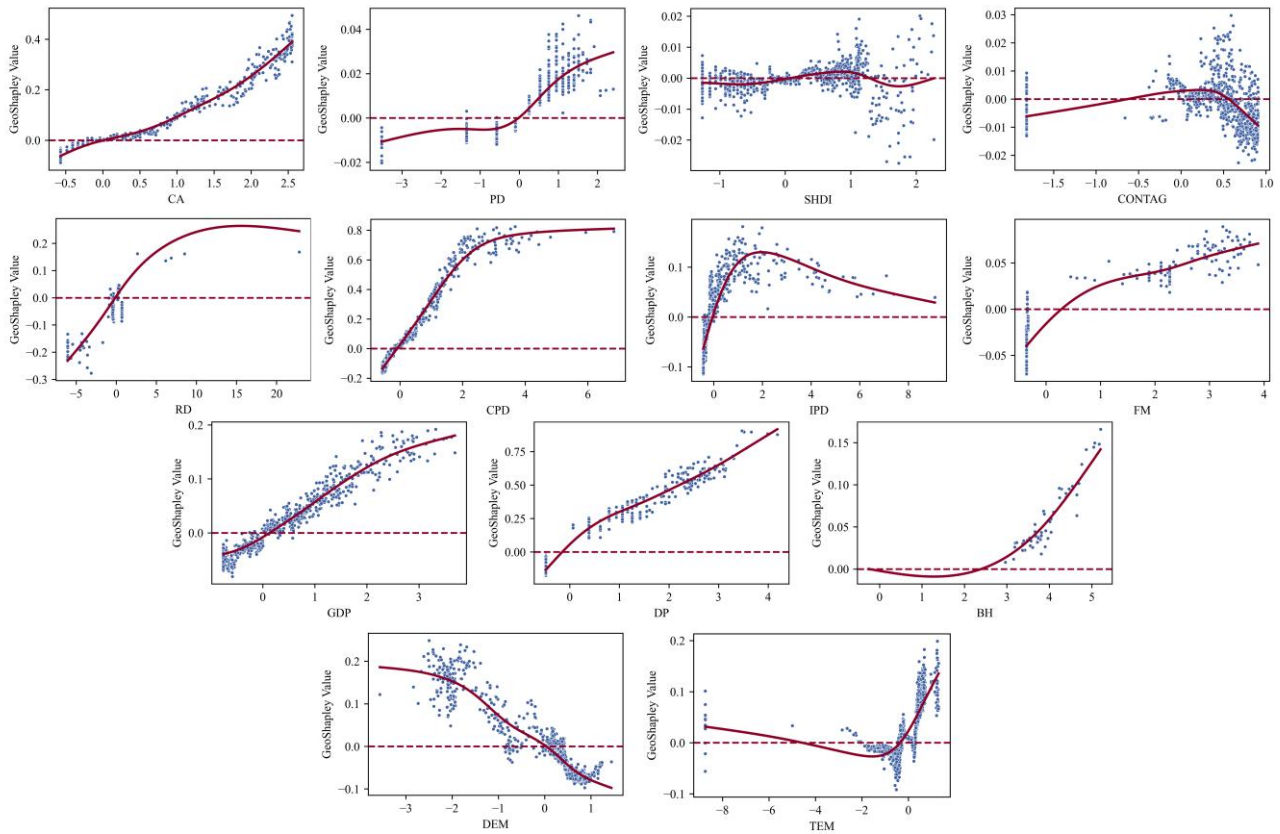


Fig.9. Marginal effects between spatial agglomeration features and their contributions to NCE.

3.4 Effects of agglomeration across natural settings

3.4.1 Contributions across climate zones

Climate zoning changed the relative contributions of different types of urban agglomeration factors. Figure 11 shows that the cold zone and the hot-summer warm-winter zone had broadly similar contribution structures, with functional spatial variables ranking high in both groups. This suggests that the clustering of commercial and industrial activities remained important for explaining NCE under different thermal conditions. By contrast, in the hot summer and cold winter zone, the contribution of social spatial agglomeration increased to 23.01%, indicating a stronger role of population-related and social activity variables. Differences among climate zones therefore lay mainly in the relative weighting of functional and social spatial variables.

Climate zoning also affected the direction and magnitude of individual variable contributions. In the cold zone, commercial spatial agglomeration was the main contributor, but the GeoShapley values of road density ranged from

-52.59% to 24.04%, indicating that transport-related variables did not have a consistent direction of effect across cities. In the hot-summer cold-winter zone, GEO contributed up to 18.71%, while the contribution of population density decreased from 55.75% to 20.12%. This change suggests that spatial location altered the explanatory power of social agglomeration variables. In other words, differences among climate zones were reflected not only in variable rankings, but also in changes in the direction and strength of individual effects.

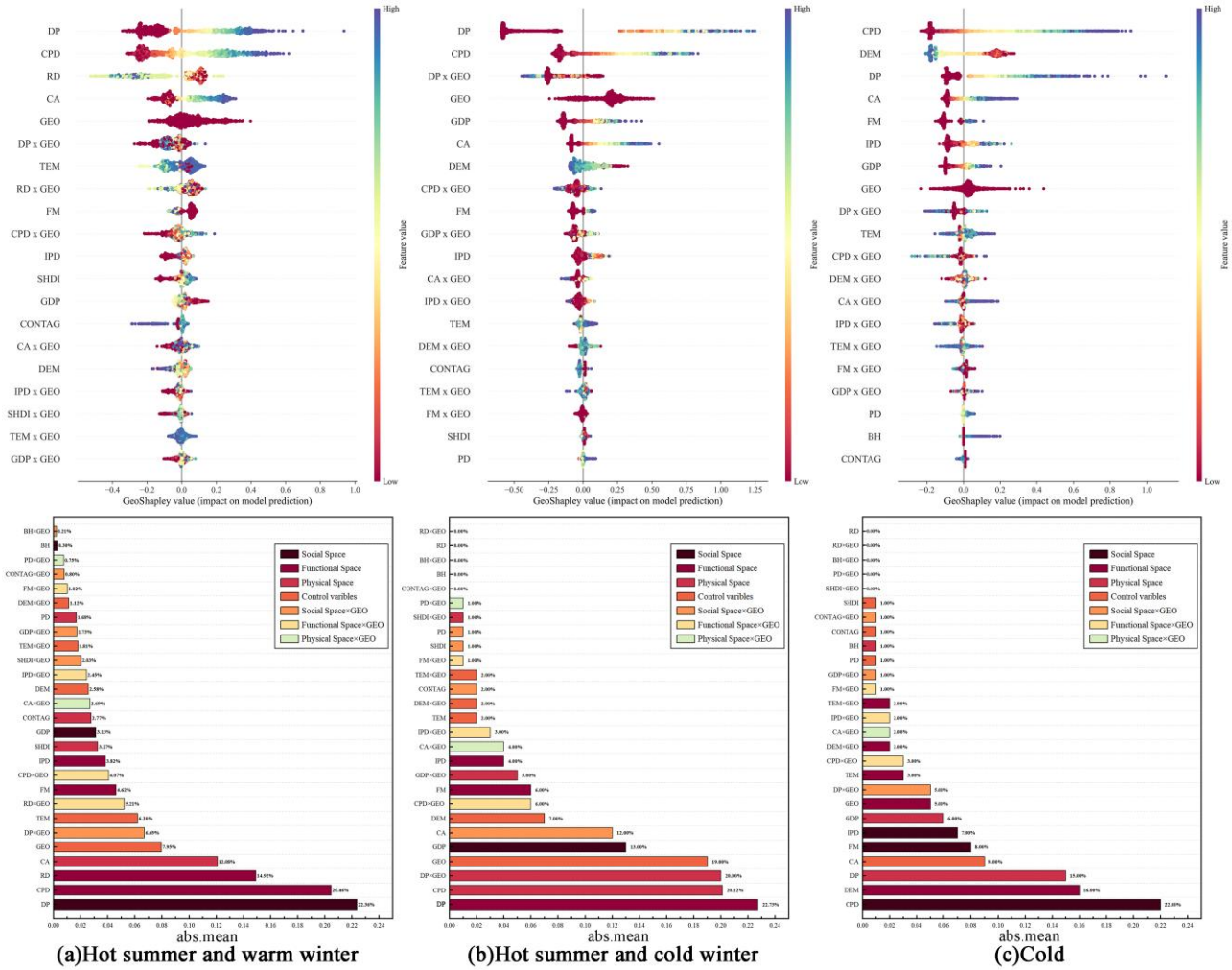


Fig.11. Spatial interpretation of feature contributions to NCE in climate zones.

3.4.2 Contributions across topographic settings

Topographic setting had a more direct effect on the contribution structure than climate zoning. Figure 12 shows that physical spatial and landscape pattern variables were more prominent in mountain cities, where CA, SHDI, and CONTAG made negative contributions to NCE. GEO contributed 6.47%, indicating that within-city location still

mattered in mountainous settings. In contrast, the contribution structure in plain cities was more strongly shaped by functional spatial variables. Where topographic constraints were weaker, the spatial organization of commercial, industrial, and other functional activities better explained differences in NCE.

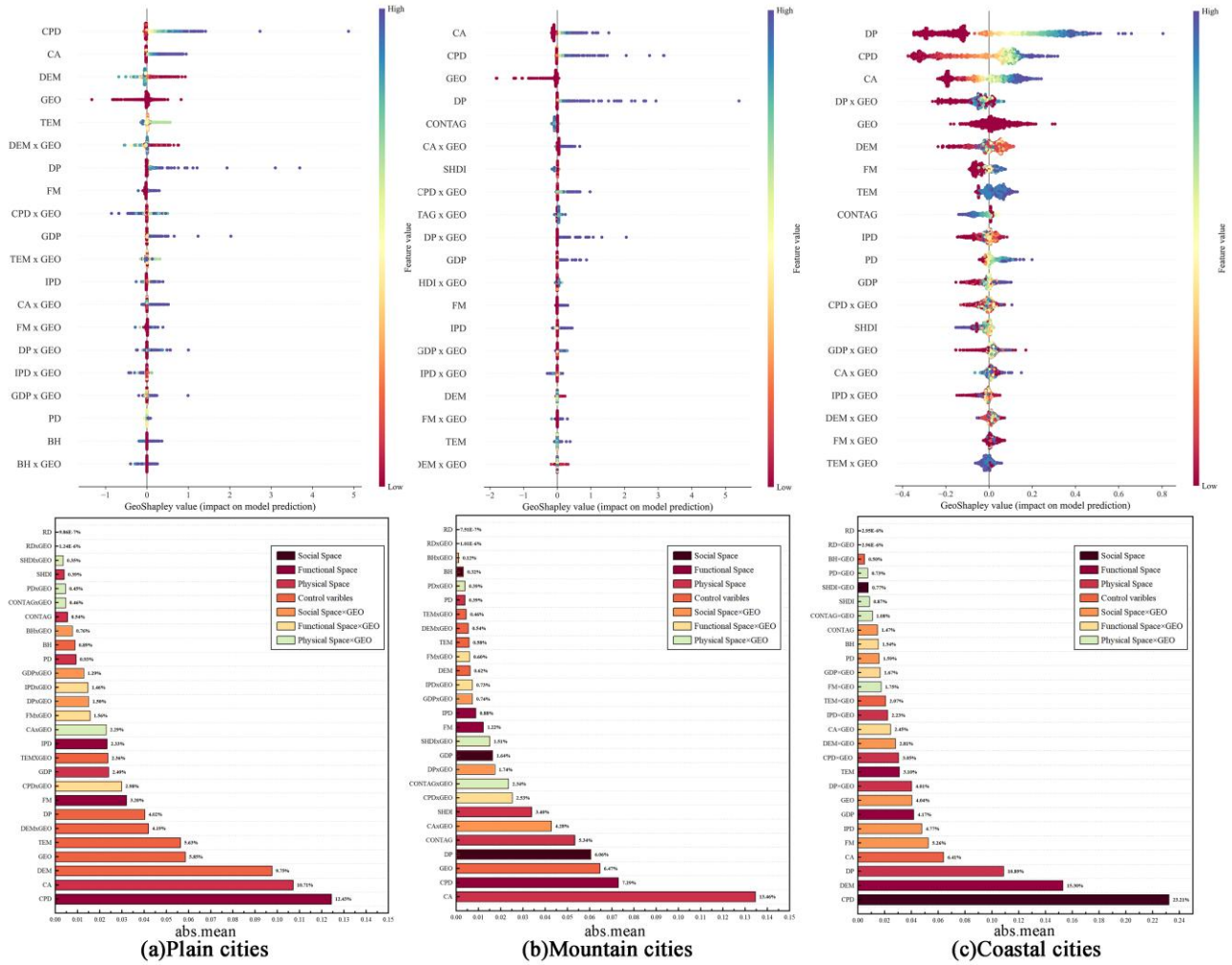


Fig.12. Spatial interpretation of feature contributions to NCE in topographic zones.

Coastal cities showed a different contribution structure, with socioeconomic spatial variables playing a more prominent role. The relationship between variables such as GDP and NCE differed from that observed in mountain and plain cities, suggesting that the effect of economic activity on net carbon emissions was conditioned by the coastal setting. Coastal cities also showed stronger differentiation between high and low NCE values, reflecting the coexistence of intensively developed areas and coastal ecological spaces. These differences indicate that mountain, plain, and coastal cities do not share a single explanatory pathway. Instead, their NCE patterns were associated,

respectively, with physical and landscape structure, functional spatial organization, and socioeconomic spatial factors.

4.Discussion

This study provides new insights into the complex relationship between urban spatial agglomeration and net carbon emissions by linking multidimensional urban structures with the spatial distribution of carbon sources and sinks. Our findings demonstrate that the carbon effects of agglomeration differ across physical, functional, and socioeconomic dimensions and vary substantially under different geographic contexts. By integrating high-resolution carbon accounting with a geographically interpretable model framework, we reveal the nonlinear and spatially heterogeneous pathways through which urban spatial organization influences carbon balance in China's megacities.

4.1 Advancing urban carbon assessment through integrated source and sink accounting

Existing urban carbon assessments have greatly improved the spatial estimation of anthropogenic emissions, but they remain largely focused on carbon sources and provide an incomplete picture of urban carbon balance. Recent studies have moved beyond traditional statistical inventories toward finer spatial assessments of urban emissions. Top-down approaches typically allocate regional emissions using energy statistics, remote sensing products, and socioeconomic data [29], whereas bottom-up approaches rely on detailed activity data to capture variations in human activities across space [30]. These approaches have improved the representation of urban emission patterns, but they mainly describe the production of carbon emissions rather than the balance between emissions and ecosystem uptake. As urban climate research increasingly considers carbon neutrality and long-term sustainability, understanding how urban spatial structures affect both carbon sources and sinks has become increasingly important. Urban spatial agglomeration influences not only energy consumption and human activity intensity, but also land use patterns and ecosystem carbon sequestration. Therefore, assessments that integrate anthropogenic emissions with ecological carbon uptake are needed to better understand the carbon consequences of urban spatial organization.

This study integrates multi-source spatial data and an interpretable modeling framework to examine urban

carbon balance from both accounting and mechanism perspectives. Previous studies have shown that combining nighttime light data with population information can improve the spatial estimation of urban energy consumption and emissions by reducing uncertainties associated with single remote sensing products [31]. Building on these advances, we combined nighttime light imagery, population density, and social sensing data to estimate anthropogenic emissions at a fine spatial scale, and further incorporated net ecosystem productivity to represent both carbon sources and sinks. Beyond improving carbon accounting, identifying the mechanisms linking urban spatial agglomeration with carbon balance requires methods that can capture both nonlinear responses and spatial variations. Spatial econometric models, such as GWR and MGWR, are effective in detecting spatially varying relationships but may not adequately capture complex nonlinear patterns. Machine learning approaches can identify nonlinear relationships but often provide limited explanations of spatial differences [32]. By combining ensemble learning with the GeoShapley framework, this study reveals how the effects of urban spatial agglomeration vary across space and provides a more detailed understanding of the factors shaping urban carbon balance.

4.2 Urban spatial organization shapes the balance between carbon sources and sinks

Urban spatial structure plays a key role in determining how carbon emissions are distributed within cities, rather than simply affecting the overall emission intensity. Classical monocentric city theories suggest that population and economic activities tend to concentrate around urban cores and gradually decline with increasing distance [33,34]. Consistent with this theoretical expectation, our results show that monocentric cities such as Beijing and Guangzhou exhibit clear center-periphery emission gradients, with emission peaks concentrated in central areas and declining rapidly toward the urban fringe (Fig. 14). This pattern reflects the concentration of energy consumption associated with intensive land use and human activities in urban cores [35]. However, as urban structures evolve from monocentric to polycentric configurations, the traditional distance-decay pattern becomes less pronounced. Multiple emission peaks observed in Shenzhen, Tianjin, and Chengdu indicate that the decentralization of employment,

industrial activities, and service functions redistributes emission hotspots across multiple urban nodes. These findings suggest that polycentric development does not necessarily reduce urban carbon emissions, but rather changes their spatial organization by redistributing population and economic activities and potentially alleviating excessive emission pressures in single urban centers [36]. In addition, Chongqing's river-oriented and clustered urban form demonstrates that topographic constraints can further modify the relationship between urban structure and emissions, generating emission hotspots beyond conventional center-periphery patterns [37].

Urban carbon sink patterns are strongly influenced by the preservation and spatial configuration of ecological spaces. Previous studies have demonstrated that rapid urban expansion transforms natural ecosystems, including forests and agricultural landscapes, into impervious surfaces, resulting in the degradation of ecosystem functions and reduced carbon sequestration capacity [38]. However, ecological carbon sequestration is not determined solely by the total amount of green space; the spatial configuration and connectivity of ecological patches also play important roles in regulating ecosystem functions [39,40]. Our results reveal that carbon sink capacity generally increases from urban centers toward peripheral areas, reflecting the ecological consequences of intensive urban development. Central areas typically contain limited ecological space because of high development intensity, whereas peripheral regions retain more natural land covers and therefore exhibit greater carbon sequestration potential. Nevertheless, this peripheral compensation pattern does not imply that carbon sinks depend only on urban fringes. The effectiveness of ecological compensation also depends on how ecological spaces are integrated within urban spatial structures. Recent studies on green infrastructure have emphasized that ecological connectivity and network configuration can enhance carbon storage capacity by improving habitat continuity and ecosystem functioning [41]. The multiple carbon sink peaks observed in some polycentric cities suggest that embedding ecological spaces among different urban nodes may facilitate more connected ecological networks and improve the spatial alignment between carbon emission areas and carbon sequestration spaces. This finding extends previous research on urban green infrastructure by suggesting that

446 the carbon benefits of ecological spaces depend not only on their extent, but also on their spatial configuration and
447 connectivity within urban landscapes.

448 **4.3 Urban spatial agglomeration has nonlinear effects on carbon outcomes across geographic**
449 **contexts**

450 The carbon effects of urban spatial agglomeration are not determined by agglomeration size alone. Instead, they
451 depend on how agglomeration reshapes resource use and the spatial organization of urban activities. Different forms
452 of agglomeration reflect different ways in which urban activities are concentrated and organized. Previous studies
453 have shown that urban density and concentration can produce both positive and negative environmental effects. On
454 the one hand, the concentration of population and economic activities involves a trade-off between increased energy
455 demand and efficiency gains from economies of scale. When additional energy consumption exceeds the benefits
456 derived from shared infrastructure and improved resource efficiency, agglomeration may intensify carbon pressures.
457 On the other hand, functional and spatial agglomeration reflects changes in how urban activities are organized. Well-
458 coordinated functional layouts and compact urban forms can reduce carbon intensity by improving infrastructure
459 sharing, minimizing spatial redundancy, and enhancing land-use efficiency, whereas poorly coordinated high-
460 intensity development may further reduce ecological spaces and weaken carbon sequestration capacity. Therefore,
461 the low-carbon potential of agglomeration does not arise from higher density alone, but from the ability of cities to
462 convert agglomeration advantages into greater resource efficiency.

463 The carbon effects of urban spatial agglomeration are also shaped by local geographical conditions, suggesting
464 that no single agglomeration pattern is universally optimal across regions. Climate conditions influence urban carbon
465 balance by affecting building energy demand and ecosystem productivity, while topography constrains urban
466 expansion and shapes spatial development patterns [42]. For example, mountainous cities often develop more
467 compact urban forms due to limited land availability while maintaining larger ecological areas, which can enhance

carbon sequestration capacity. By contrast, plain and coastal cities generally have greater capacity for urban expansion but face stronger conflicts between development pressure and ecological conservation [43]. Therefore, the carbon effects of urban spatial agglomeration emerge from the interaction between urban development processes and geographical constraints.

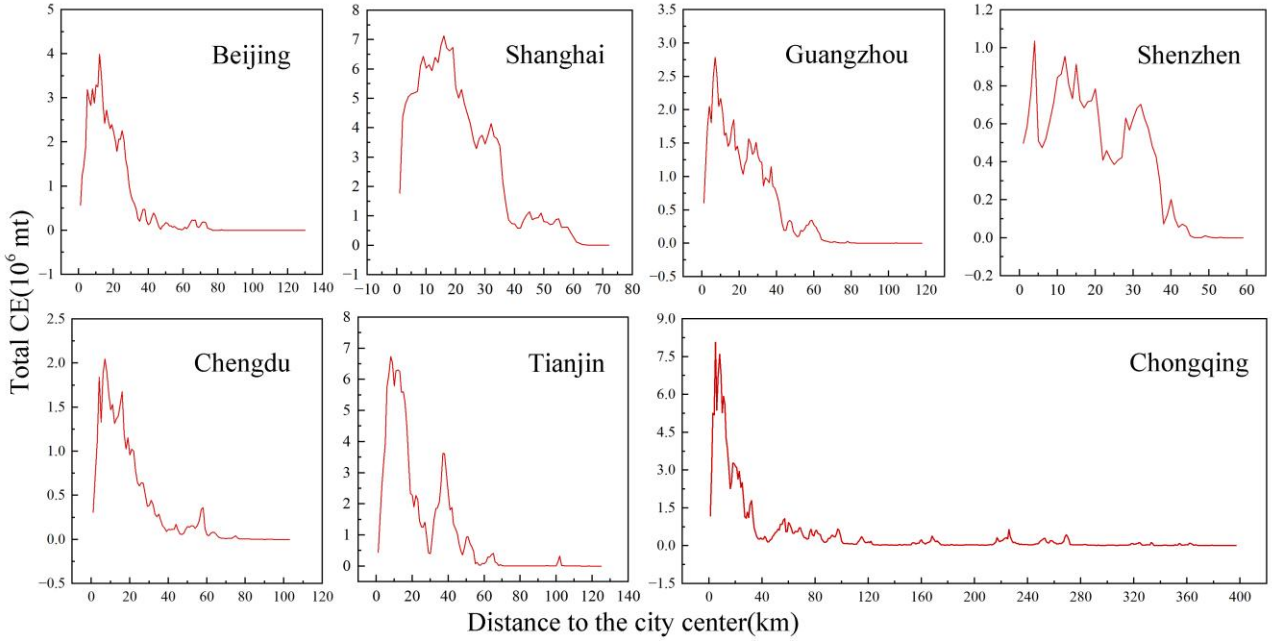


Fig.13. Spatial gradients of carbon emissions in China's megacities.

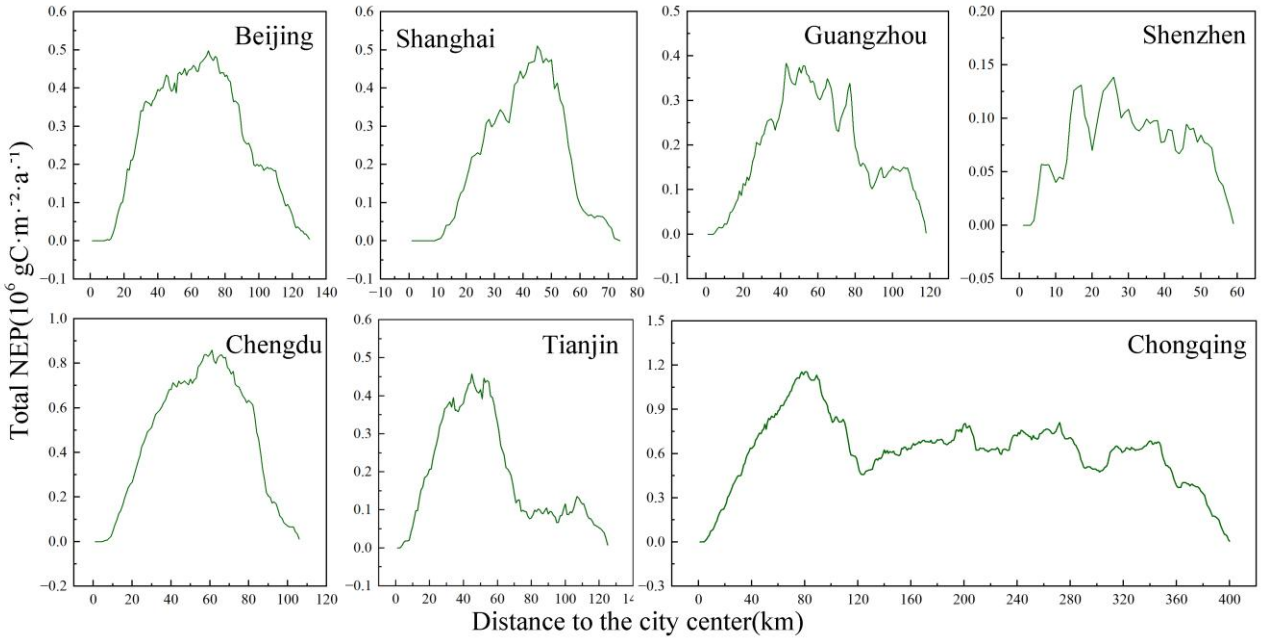


Fig.14. Spatial gradients of carbon sink in China's megacities

4.4 Implications for climate-sensitive urban planning

The findings highlight that low-carbon planning in megacities should move beyond a simple pursuit of higher density and instead focus on optimizing the relationship between spatial agglomeration, ecological capacity, and geographical conditions. Three policy implications are proposed.

First, urban spatial agglomeration should be guided toward higher efficiency rather than continued expansion. Compact development should not be regarded as a universal low-carbon solution, as its environmental benefits depend on how effectively cities coordinate population distribution, functional organization, and infrastructure provision Future urban renewal should therefore prioritize improving the spatial alignment of employment, housing, transportation, and public services, while avoiding excessive intensification in already constrained urban cores.

Second, carbon governance should integrate emission reduction with the enhancement of ecological sinks. Rather than focusing solely on controlling emissions within built-up areas, planning strategies should strengthen the connection between urban development and ecological systems. Protecting continuous ecological spaces, improving blue-green infrastructure networks, and enhancing ecological connectivity can help increase carbon sequestration capacity while reducing the imbalance between urban carbon sources and sinks.

Third, low-carbon strategies should be adapted to local geographical conditions. Different urban environments require differentiated planning approaches. For example, mountain cities should prioritize ecological conservation and development control in environmentally sensitive areas, while plain and coastal cities should better coordinate urban expansion with ecological protection. Climate-responsive planning, including reducing building energy demand in colder regions and enhancing cooling and ventilation capacity in warmer regions, should also be incorporated into long-term low-carbon urban strategies.

5. Conclusions

This study integrates multi-source geospatial data to develop a spatially explicit estimate of urban net carbon

emissions and applies an interpretable machine learning framework to uncover how urban spatial agglomeration shapes carbon patterns across megacities. Three major findings emerge:

First, Chinese seven megacities exhibit a spatial mismatch between carbon emissions and carbon sequestration, with emissions concentrated in urban cores and carbon sinks primarily distributed in peripheral ecological spaces.

Second, urban spatial agglomeration has nonlinear effects on net carbon emissions, and these effects differ across dimensions. Socioeconomic and functional clustering show stronger associations with net carbon emissions than urban morphology.

Third, the carbon effects of urban agglomeration vary across geographic contexts, with climate and topography further shaping the relationship between spatial agglomeration and urban carbon balance.

This study has several limitations. First, the cross-sectional design limits our ability to capture the long-term dynamics between changes in urban agglomeration and carbon responses. Future studies should incorporate longitudinal datasets and dynamic models to examine the lagged effects of planning interventions. Second, although the 500 m spatial resolution balances computational efficiency and spatial detail, scale effects may influence the observed relationships and should be further evaluated through multi-scale analyses. Finally, this study mainly focuses on the roles of spatial agglomeration and natural conditions, while socioeconomic factors such as economic restructuring, industrial transformation, and governance capacity remain insufficiently explored. Future research should integrate both environmental and socioeconomic processes to better understand pathways toward low-carbon urban transformation under diverse development contexts.

‘Declaration of generative AI and AI-assisted technologies in the writing process’:

During the preparation of this work, the author(s) used [ChatGPT] in order to [English editing and grammar checks]. After using this tool/service, the author(s) reviewed and edited the content as needed and take full responsibility for the content of the publication.

Declaration of Consent to Publish

Not applicable.

Declaration of Funding

This study was supported by National Natural Science Foundation of China (NO. 52278059), Financially supported by National Key R&D Program of China (No. 2024YFC3808500).

Declaration of Ethics and Consent to Participate

Not applicable.

Availability of data and materials

The data that support the findings of this study are available from the corresponding author upon reasonable request.

Author's contributions:

Yan Chen: Conceptualization, Methodology, Formal analysis, Writing - original draft, Writing - review & editing ; Sheng Jiao: Supervision, Validation, Funding acquisition, Writing - review & editing ; Zongcai Wei: Investigation, Writing - review & editing ; Xinyue Gu: Investigation, Visualization.

Declaration of competing interest

The authors declare that they have no known competing financial interests or personal relationships that could have appeared to influence the work reported in this paper.

References

1. Esch T, Heldens W, Hirner A, Keil M, Marconcini M, Roth A, et al. Breaking new ground in mapping human settlements from space – The Global Urban Footprint. ISPRS Journal of Photogrammetry and Remote Sensing. 2017; 134:30–42. https://doi.org/10.1016/J.ISPRSJPRS.2017.10.012.

2. Kikstra JS, Nicholls ZRJ, Smith CJ, Lewis J, Lamboll RD, Byers E, et al. The IPCC Sixth Assessment Report WGIII climate assessment of mitigation pathways: from emissions to global temperatures. Geosci Model Dev.

2022; 15:9075–109. https://doi.org/10.5194/GMD-15-9075-2022.

3. Zhu Y, Zhang Y, Zhang Y, Zheng B. Tracing CO2 emissions across megacity landscapes: beyond citywide totals to structural heterogeneity and mitigation. Environmental Science and Ecotechnology. 2025; 27:100602. https://doi.org/10.1016/J.ESE.2025.100602.

4. Lu J, Li B, Li H, Al-Barakani A. Expansion of city scale, traffic modes, traffic congestion, and air pollution. Cities. 2021;108. https://doi.org/10.1016/j.cities.2020.102974.

5. Xiang W, Lan Y, Gan L, Li J. How does new urbanization affect urban carbon emissions? Evidence based on spatial spillover effects and mechanism tests. Urban Clim. 2024; 56:102060. https://doi.org/10.1016/J.UCLIM.2024.102060.

6. Li L, Sun S, Pang Z, Dong L, Han J, Qian X. Uncovering nonlinear threshold effects of urban morphology on carbon emissions: Toward optimal low-carbon urban spatial planning. Cities. 2026; 171:106831. https://doi.org/10.1016/J.CITIES.2026.106831.

7. Wang SH, Huang SL, Huang PJ. Can spatial planning really mitigate carbon dioxide emissions in urban areas? A case study in Taipei, Taiwan. Landsc Urban Plan. 2018; 169:22–36. https://doi.org/10.1016/J.LANDURBPLAN.2017.08.001.

8. Wang Y, Zhang D, He C, Qi T, Li P. Simulating the effects on carbon sinks caused by urban expansion using a coupled urban–ecological model. J Clean Prod. 2025; 520:146184. https://doi.org/10.1016/J.JCLEPRO.2025.146184.

9. Hao Y, Cho HC. Research on the relationship between urban public infrastructure, CO2 emission and economic growth in China. Environ Dev Sustain. 2022; 24:7361–76. https://doi.org/10.1007/S10668-021-01750-0/FIGURES/4.

10. Zhou B, Rybski D, Kropp JP. The role of city size and urban form in the surface urban heat island. Sci Rep. 2017;

7:1–9. https://doi.org/10.1038/S41598-017-04242-2.

11. Ji Y, Liu Y, Tang H, Li Z, Bai Y, Feng T. Stratified strategies for enhancing thermal comfort through multidimensional compactness optimization in urban built-up areas during heatwaves. Sustain Cities Soc. 2025; 127:106445. https://doi.org/10.1016/J.SCS.2025.106445.

12. Zagow M. Does mixed-use development in the metropolis lead to less carbon emissions? Urban Clim. 2020; 34. https://doi.org/10.1016/j.uclim.2020.100682.

13. Xiaoxu X, Qiangmin X, Weihao S. Impact of urban compactness on carbon emission in Chinese cities: From moderating effects of industrial diversity and job-housing imbalances. Land use policy. 2024; 143:107213. https://doi.org/10.1016/J.LANDUSEPOL.2024.107213.

14. Li Q, Yang X, Lin T. Polycentric urban development and carbon emission Intensity——An examination of 268 Chinese cities. J Clean Prod. 2025; 510:145599. https://doi.org/10.1016/J.JCLEPRO.2025.145599.

15. Kang T, Wang H, He Z, Liu Z, Ren Y, Zhao P. The effects of urban land use on energy-related CO2 emissions in China. Science of The Total Environment. 2023; 870:161873. https://doi.org/10.1016/J.SCITOTENV.2023.161873.

16. Naveed A, Ahmad N, FathollahZadeh Aghdam R, Menegaki AN. What have we learned from Environmental Kuznets Curve hypothesis? A citation-based systematic literature review and content analysis. Energy Strategy Reviews. 2022; 44. https://doi.org/10.1016/j.esr.2022.100946.

17. Zhang J, Xie Y, Luan B, Chen X. Urban macro-level impact factors on Direct CO2 Emissions of urban residents in China. Energy Build. 2015; 107:131–43. https://doi.org/10.1016/j.enbuild.2015.08.011.

18. Zhang X, Meng Q, Xu J, Li K. Urbanization impacts on anthropogenic carbon dioxide emissions and the roles of urban morphologies: Insights from urban socioeconomic clusters and local climate zones in Shanghai, China. Sustain Cities Soc. 2025; 129:106494. https://doi.org/10.1016/J.SCS.2025.106494.

582 19. Shi Y, Zhang B, Liang L, Wang S, Zhang H, Sun H, et al. Unfolding the effectiveness of ecological restoration
583 programs in enhancing vegetation carbon sinks across different climate zones in China. Resour Conserv Recycl.
584 2025; 212:107974. https://doi.org/10.1016/J.RESCONREC.2024.107974.
585 20. Zhao D, Cai J, Shen S, Liu Q, Lan Y. Nature-based solutions: Assessing the carbon sink potential and influencing
586 factors of urban park plant communities in the temperate monsoon climate zone. Science of the Total
587 Environment. 2024; 950. https://doi.org/10.1016/j.scitotenv.2024.175347.
588 21. Zhao C, Liu J, Mou W, Zhao W, Zhou Z, Ta F, et al. Topography shapes the carbon allocation patterns of alpine
589 forests. Science of The Total Environment. 2023; 898:165542.
590 https://doi.org/10.1016/J.SCITOTENV.2023.165542.
591 22. Wu Y, Shi K, Li X, Ru Y. Recovery of economic activities in China uncovered by remotely sensed nighttime light
592 data under the pandemic new normal. Applied Geography. 2025; 175.
593 https://doi.org/10.1016/j.apgeog.2025.103506.
594 23. Wu W Ben, Ma J, Banzhaf E, Meadows ME, Yu ZW, Guo FX, et al. A first Chinese building height estimate at
595 10 m resolution (CNBH-10 m) using multi-source earth observations and machine learning. Remote Sens
596 Environ. 2023; 291. https://doi.org/10.1016/j.rse.2023.113578.
597 24. Nemani RR, Keeling CD, Hashimoto H, Jolly WM, Piper SC, Tucker CJ, et al. Climate-driven increases in global
598 terrestrial net primary production from 1982 to 1999. Science (1979). American Association for the
599 Advancement of Science; 2003; 300:1560–3. https://doi.org/10.1126/SCIENCE.1082750.
600 25. Tang Z, Wang Y, Fu M, Xue J. The role of land use landscape patterns in the carbon emission reduction: Empirical
601 evidence from China. Ecol Indic. 2023; 156:111176. https://doi.org/10.1016/J.ECOLIND.2023.111176.
602 26. Jedwab R, Barr J, Brueckner JK. Cities Without Skylines: Worldwide Building-Height Gaps and their Possible
603 Determinants and Implications. J Urban Econ. 2022; 132:103507. https://doi.org/10.1016/J.JUE.2022.103507.

27. Code for design of civil buildings GB 50352-2005.

28. Li Z. GeoShapley: A Game Theory Approach to Measuring Spatial Effects in Machine Learning Models. Ann Am Assoc Geogr. 2024; 114:1365–85. https://doi.org/10.1080/24694452.2024.2350982.

29. Wang L, Fan H, Wang Y. Improving population mapping using Luojia 1-01 nighttime light image and location-based social media data. Science of the Total Environment. 2020; 730. https://doi.org/10.1016/j.scitotenv.2020.139148.

30. Yao Y, Liu X, Li X, Zhang J, Liang Z, Mai K, et al. Mapping fine-scale population distributions at the building level by integrating multisource geospatial big data. International Journal of Geographical Information Science. 2017; 31:1220–44. https://doi.org/10.1080/13658816.2017.1290252.

31. Guo B, Xie T, Zhang W, Wu H, Zhang D, Zhu X, et al. Rasterizing CO2 emissions and characterizing their trends via an enhanced population-light index at multiple scales in China during 2013–2019. Science of The Total Environment. 2023; 905:167309. https://doi.org/10.1016/J.SCITOTENV.2023.167309.

32. Foroutan E, Hu T, Li Z. Revealing key factors of heat-related illnesses using geospatial explainable AI model: A case study in Texas, USA. Sustain Cities Soc. 2025; 122:106243. https://doi.org/10.1016/J.SCS.2025.106243.

33. Zhang T, Sun B, Li W. The economic performance of urban structure: From the perspective of Polycentricity and Monocentricity. Cities. 2017; 68:18–24. https://doi.org/10.1016/J.CITIES.2017.05.002.

34. Wei Z, Huang W, Tang Q, Xie R. Spatial Heterogeneities of O2O Retail Space in Urban China Under Digital Transformation: Evidence from Guangzhou, China. Chinese Geographical Science 2025 35:5. 2025; 35:963–81. https://doi.org/10.1007/S11769-025-1493-6.

35. Zheng M, Huang W, Xu G, Li X, Jiao L. Spatial gradients of urban land density and nighttime light intensity in 30 global megacities. Humanit Soc Sci Commun. 2023; 10:1–11. https://doi.org/10.1057/S41599-023-01884-8.

36. Chen Z, Li Q, Su H. Do the urban polycentricity and dispersion affect multisectoral carbon dioxide emissions? A

626 case study of 95 cities in southeast China based on nighttime light data. Int J Digit Earth. 2023; 16:4867–84.
627 https://doi.org/10.1080/17538947.2023.2288151.
628 37. Qiu L, Niu K, He W, Hu Y. Two Contribution Paths of Carbon Neutrality: Terrestrial Ecosystem Carbon Sinks
629 and Anthropogenic Carbon Emission Reduction—A Case of Chongqing, China. Sustainability. 2023; 15:11306.
630 https://doi.org/10.3390/SU151411306.
631 38. Wei G, He BJ, Liu Y, Li R. How does rapid urban construction land expansion affect the spatial inequalities of
632 ecosystem health in China? Evidence from the country, economic regions and urban agglomerations. Environ
633 Impact Assess Rev. 2024; 106:107533. https://doi.org/10.1016/J.EIAR.2024.107533.
634 39. Forman RTT. Some general principles of landscape and regional ecology. Landsc Ecol. 1995; 10:133–42.
635 https://doi.org/10.1007/BF00133027/METRICS.
636 40. Zhao J, Li Z, Wu J, Xu Z, Ja B. Ecological spatial network optimization of carbon sink patches for enhanced
637 carbon sink in Wuhan Metropolitan Area, China. Ecol Indic. 2024; 165:112177.
638 https://doi.org/10.1016/J.ECOLIND.2024.112177.
639 41. Zhang Y, Kong W, Wang G. The impact of green infrastructure on ecosystem quality based on explainable
640 machine learning: a case study of Shanxi Province, China. Scientific Reports. 2025; 15:31295-.
641 https://doi.org/10.1038/s41598-025-17261-1.
642 42. Li Z, Nie M. Research on the Characteristics and Evolution of Urban Spatial Structures under Complex Terrain
643 Conditions: Taking 71 Typical Cities in China as an Example. J Urban Plan Dev. 2024; 150:04024019.
644 https://doi.org/10.1061/JUPDDM.UPENG-4735.
645 43. Jing T, Wang H, Yang Y, Jin Y, Yu W, Zhong Y. Achieving sustainable development in coastal cities: Exploring
646 the synergies between urban resilience and high-quality development. Sustain Cities Soc. 2026; 136:107112.
647 https://doi.org/10.1016/J.SCS.2025.107112.

648

Supplementary Files

This is a list of supplementary files associated with this preprint. Click to download.

- Thesupplementarymaterial.docx